Title

Injectable polyethylene glycol-laponite composite hydrogels as articular cartilage scaffolds with superior mechanical and rheological properties

Journal

International Journal of Polymeric Materials, 66(3)

ISSN

0091-4037

Authors

Nojoomi, Amirali
Tamjid, Elnaz
Simchi, Abdolreza
et al.

Publication Date

2017-02-11

DOI

10.1080/00914037.2016.1182914

Peer reviewed

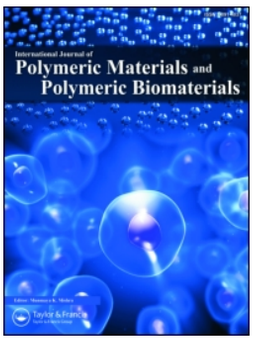

International Journal of Polymeric Materials and Polymeric Biomaterials

ISSN: 0091-4037 (Print) 1563-535X (Online) Journal homepage: http://www.tandfonline.com/loi/gpom20

Injectable polyethylene glycol-laponite composite hydrogels as articular cartilage scaffolds with superior mechanical and rheological properties

Amirali Nojoomi, Elnaz Tamjid, Abdolreza Simchi, Shahin Bonakdar & Pieter Stroeve

To cite this article: Amirali Nojoomi, Elnaz Tamjid, Abdolreza Simchi, Shahin Bonakdar & Pieter Stroeve (2017) Injectable polyethylene glycol-laponite composite hydrogels as articular cartilage scaffolds with superior mechanical and rheological properties, International Journal of Polymeric Materials and Polymeric Biomaterials, 66:3, 105-114, DOI: 10.1080/00914037.2016.1182914

To link to this article: http://dx.doi.org/10.1080/00914037.2016.1182914

Accepted author version posted online: 11 May 2016.
Published online: 11 May 2016.

INTERNATIONAL JOURNAL OF POLYMERIC MATERIALS AND POLYMERIC BIOMATERIALS
2017, VOL. 66, NO. 3, 105–114
http://dx.doi.org/10.1080/00914037.2016.1182914

Taylor & Francis
Taylor & Francis Group

Injectable polyethylene glycol-laponite composite hydrogels as articular cartilage scaffolds with superior mechanical and rheological properties

Amirali Nojoomi[a], Elnaz Tamjid[b], Abdolreza Simchi[a,c], Shahin Bonakdar[d] and Pieter Stroeve[e]

[a]Department of Materials Science and Engineering, Sharif University of Technology, Tehran, Iran; [b]Department of Nanobiotechnology, Faculty of Biological Sciences, Tarbiat Modares University, Tehran, Iran; [c]Institute for Nanoscience and Nanotechnology, Sharif University of Technology, Tehran, Iran; [d]National Cell Bank of Iran, Pasteur Institute of Iran, Tehran, Iran; [e]Department of Chemical Engineering, University of California Davis, Davis, California

ABSTRACT

In this study, injectable PEG-based hydrogels containing Laponite particles with mechanical and structural properties close to the natural articular cartilage are introduced. The nanocomposites are fabricated by imide ring opening reactions utilizing synthesized copolymers containing PEG blocks and nanoclay through a two-step thermal poly-(amic acid) process. Butane diamine is used as nucleophilic reagent and hydrogels with interconnected pores with sizes in the range of 100–250 µm are prepared. Improved viscoelastic properties compared with the conventional PEG hydrogels are shown. Evaluation of cell viability utilizing human mesenchymal stem cells determines cytocompatibility of the nanocomposite hydrogels.

GRAPHICAL ABSTRACT

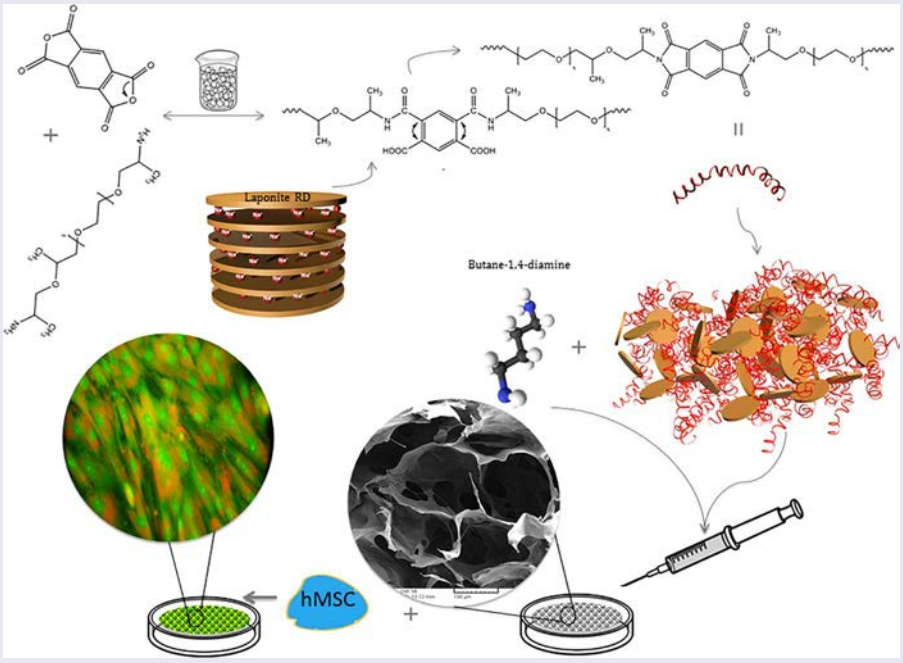

ARTICLE HISTORY
Received 18 December 2015
Accepted 22 April 2016

KEYWORDS
Hydrogels; nanoclay; polyethylene glycol; rheology; cartilage tissue engineering

1. Introduction

Articular cartilage as a highly specialized connective tissue of diarthrodial joints has to deliver a low friction surface to enable the transmission of the applied loads on the joint [1]. Lack of blood vessels, lymphatics, and nerves as well as a harsh biomechanical environment limit articular cartilage's ability for intrinsic healing and repair. Hydrogels have an ability to withstand high cyclic loads by the incorporation of pressurized water within the matrix combined with the network resistance to water flow; they have long received attention in the fields of biotechnology, tissue engineering and drug delivery applications because of their hydrophilic character and structural similarities to extracellular matrix [2]. Crosslinked poly-(ethylene glycol) (PEG) hydrogels are the most applicable hydrogels in regenerative medicine and tissue engineering. For example, photocrosslinking of PEG hydrogels is used to encapsulate

CONTACT Abdolreza Simchi simchi@sharif.edu Department of Materials Science and Engineering, Sharif University of Technology, Tehran, Iran.
Color versions of one or more of the figures in the article can be found online at www.tandfonline.com/gpom.

cells or used as a mediator in the immobilization of the RGD sequence [2]. Particularly, PEG hydrogels have been successfully used as stem cell delivery vehicles for cartilage growth *in vivo* and used as chondrocyte cell carriers to generate cartilaginous tissue for tissue engineering [3–5].

PEG acrylates are a major type of macromeres used for polymerization hydrogels by free-radical methods. Besides their simplicity, suitable biocompatibility, nonimmunogenity, and protein adsorption resistance, these reactions often limit the controllability of network structures while they are not naturally degradable [5,6]. A recent study [7] showed that PEGylated parts made by the free-radical method cause specific clinical, biochemical, and histologic risk factors such as immune-mediated graft dysfunction. Furthermore, PEG-based hydrogels prepared by free-radical methods with low density of crosslinking sites often lack appropriate mechanical properties, which limit their application for bioactive cell delivery approach or soft tissue repair [8]. To overcome these limitations, researchers have focused on preparing multifunctional precursors with active groups as crosslinking sites to enhance the crosslinking density of PEG networks [9]. Shao et al. [10] introduced amine dendrimers as crosslinking agents for polyimide membranes for gas separation purposes. Sun et al. [11] used this method for the synthesis of PEG-based hydrogels by crosslinking multifunctional copolymers. The imide ring opening method offers significant advantages over traditional processing methods of polymer networks as they form rapidly under ambient conditions without free-radical initiators and catalysis [10–12]. This method provides single PEG chains with a high number of crosslinking sites, which not only improves mechanical and structural properties and controllability of the network but also offers active amide sites that can be used for conjugating protein-based drugs [13,14].

Chemical and physical crosslinking can be afforded to increase the density of crosslinking sites and thus improve the mechanical properties. Physical crosslinking by bioactive reinforcement particles is a novel approach to enhance mechanical properties by increasing chain entanglement sites while increasing cell attachment and proliferation [15,16]. Different reinforcement particulates such as bioactive glass [17], carbon nanotubes [18], hydroxyapatite [19], and nanoclays [20–22] have been utilized. Nelson and Cosgrove [23,24] showed that PEG chains readily adhere to Laponite surfaces and increase physical entanglement. Gaharwar et al. [25,26] showed that the dispersion of Laponite particles in the PEG network enhances mechanical properties with improved cell adhesion and proliferation. The exfoliation of Laponite in the polymer matrix yields high surface area, which reduces the energy of cell proliferation on the surface of clays providing strong cell affinity. However, if particle lamellas form stacks, free basal surface as an active site for cell attachment tend to decrease [27].

Injectable hydrogels have received much attention over preformed implantations because of their minimally invasive nature and the ability to fill any cavity or defect. Many of the reported injectable gels are actually liquids that once injected undergo a sol–gel phase transition or *in situ* polymerization [28]. The various triggers that have been utilized to induce an *in vivo* sol–gel transition including salt [29], temperature [30,31], enzymes [32], and photo-initiated polymerization [33]. Despite its many advantages, conventional systems for obtaining injectable hydrogels have some major drawbacks. For instance, there is a high potential for leakage of the gel precursor to unwanted sites before the onset of the sol–gel phase transition [28,34]. Moreover, using free-radical methods may have some specific clinical, biochemical, and histologic risk factors [7].

In this study, a PEG-based copolymer with multifunctional imide groups was synthesized through a two-step poly-(amic acid) process to form an injectable precursor. This can be highly crosslinked via an amine nucleophile to form a strong hydrogel under ambient temperature without using catalysis and free-radical initiators. It is shown that the addition of highly exfoliated silicate nanoparticles to the PEG chains during polyimide synthesis significantly improve the rheological behavior of the injectable precursor. A remarkable influence on the storage modulus was observed, which can make the scaffold be able to withstand the normal loads and stresses of native cartilage (type II collagen), in the initial stages and before the cells begin producing functional ECM. The exclusive property combinations of the hydrogels show that new approaches to engineering complex injectable hydrogels, which may be applied in applications that need higher modulus than conventional ones. The presence of active imide groups as chemical crosslinking sites on each synthesized polymers may also provide the ability of introducing drugs to the main chain of the synthesized hydrogel. Especially protein-based drugs can be conjugated to the polymer chain precursor through the site-directed reaction with the unpaired cysteine [35]. The high storage modulus combined with injectability and providing ability for conjugating protein-based drugs has made this system an ideal substitute for current commercial injectable scaffolds.

2. Experimental

2.1. Materials

Two types of amino-terminated poly-(ethylene glycol) (ATPEG) with a molecular weigh of 600 and 900 g.mol^{-1} were kindly provided by Hundsman Corporation (USA). Pyromellitic dianhydride (PMDA; purity 97%) and 1-methyl-2-pyrrolidinone(NMP; purity +99%) were purchased from Alfa Aesar (USA). Medical grade hectorite-type synthetic silicate powder (Laponite RD) with a chemical composition of $Na^{+}_{0.7}\left[\left(Si_8Mg_{5.5}Li_{0.3}\right)O_{20}(OH)_4\right]^{-}_{0.7}$, was purchased from Southern Clay Products Inc (USA). For the preparation of simulated body fluid (SBF) and phosphate-buffered saline (PBS) solutions, sodium chloride (NaCl; purity 99.5%), sodium bicarbonate ($NaHCO_3$; purity 99.5%), potassium chloride (KCl; purity 99.5%), hydrated dipotassium phosphate ($K_2HPO_4.3H_2O$; purity 99%), monopotassium phosphate (KH_2PO_4; purity 99%), hydrated magnesium chloride ($MgCl_2.6H_2O$; purity 98%), calcium chloride ($CaCl_2$; purity 99%), sodium sulfate (Na_2SO_4; purity 99%), tris(hydroxymethyl)amino methane ($(HOCH_2)_3CNH_2$; 99.9%), and hydrochloric acid (HCl; 1 kmol.m^{-3}) were provided by Merck, Germany.

2.2. Synthesis of PEG-based precursor and hydrogel

A typical two-step poly(amic acid) thermal procedure for polyimide synthesis was used to obtain PEG-based linear block copolymers from two different PEG linear blocks. Figure 1a shows a schematic of the used procedure. ATPEG was poured into 1-methyl-pyrrolidinone and vigorously stirred at 0°C for 10 min. An equivalent molar of PMDA was gradually added to the ATPEG solution to initiate the formation of poly-(amic acid). To stabilize the intermediate phase, the mixture was held for 60 min and then warmed up to 35°C. After magnetic stirring under a high purity nitrogen atmosphere for 8 h, a two-step thermal cycling at 140°C/6 h and 180°C/4 h was conducted. Finally, the batch was let to cool down slowly to ambient temperature. For purification, the polyimide copolymer was precipitated by diethyl ether, washed for three times, dried at room temperature for one day, and finally vacuum dried at 80°C for 4 h. In order to prepare PEG-based hydrogels, the purified copolymers were dissolved in PBS (30 wt%) under sonication (600 W, WUC – D10H, Wiseclean, Germany) for 30 min. A predetermined amount of Butane diamine (BDA) was added at room temperature to initiate the formation of crosslinking sites via imide ring opening procedure (Figure 1b). The amount of BDA was determined from gel permeation chromatography (GPC) as will be discussed in the next section.

2.3. Synthesis of PEG-based nanocomposite

For the preparation of Laponite-PEG nanocomposite, the silicate nanoparticles were added to ATPEG during the synthesis of poly-(amic acid) under vigorous stirring. Previous studies have revealed that the addition of 1–5 wt% Laponite can significantly increase the mechanical properties and cell proliferation ability of the PEG-based scaffolds [25,26]. However, during the *in situ* formation of PEG-based chains, high content of particles would impede the processability by reducing the mobility of reactants and making the reaction diffusion control. Furthermore, using high solid loading would decrease the injectability by increasing the viscosity of the precursor. Considering all these factors, the weight ratio of Laponite to the final PEG copolymer was taken to be 2.5 wt%. Both ATPEG precursors with different molecular weight were utilized to synthesize the nanocomposites. Samples were named according their molecular weights and Laponite content. PEG600 and PEG900 correspond to samples with no Laponite content with intermediate PEG chain blocks of 600 and 900 g. mol^{-1}, respectively. PEG600-2.5%L and PEG900-2.5%L are the same samples with 2.5 wt% Laponite content.

2.4. Materials characterization

Formation of the polyimide copolymer was demonstrated by 13-Carbon nuclear magnetic resonance (^{13}C-NMR, AVANCE III, Bruker) using DCM as a solvent. Gel permeation chromatography with multiangle laser light scattering (GPC, Varian ProStar) was used to determine the average molecular weights (M_n) and the polydispersity index (PDI) of the synthesized copolymers. Wide- and small-angle XRD measurements were made in the reflection mode with an Xpert Pro MPD, with a Cu anode ($K_\alpha = 0.1542$ nm) and with step size $2\theta = 0.026°$. The wide-angle XRD measurement was conducted in the interval of $5.01° < 2\theta < 79.97°$ while the small-angle one was examined in the range of $1.01° < 2\theta < 9.97°$. The Laponite clays were analyzed as powders after dispersion in DI water and subsequent drying for 24 h. Hydrogel nanocomposites were gel casted into disks with 2 mm thickness and 20 mm diameter. Samples for the XRD analysis were prepared under an applied pressure of ~80 Pa in order to align clay's basal surfaces and intensify (00 l) peaks in the pattern.

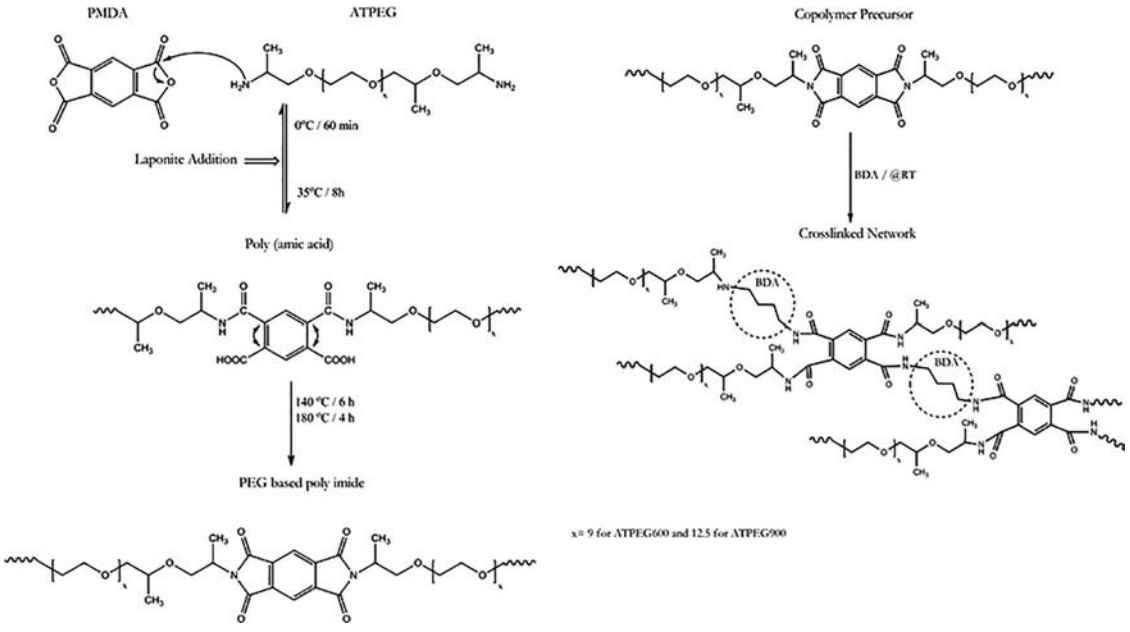

Figure 1. Schematic drawings show the procedure used to prepare PEG-based precursors and hydrogels. (a) Two-step poly-(amic acid) thermal procedure. (b) Ring opening reaction of maleimide groups during crosslinking. Symbol "x" denotes the number of PEG linear blocks, which is 9 and 12.5 for ATPEG600 and ATPEG900, respectively.

Zeta potential of PEG900 containing 2.5%L nanoparticles was measured using a ZC-2000 Microtec instrument (Microtec Inc, USA) at 25 ± 1°C. The potential was determined from the mobility of the particles using the Smoluchowski equation [36]. The test was performed on the composite precursor prepared by mechanical mixing and ultra sounding either during in situ synthesis. The specimens were dispersed in PBS at a concentration of 2 g/L. Rheological properties of the gelcast precursors were investigated using a Modular Compact rheometer (MCR 300, Anton Paar GmbH, Austria) at 25°C, with a Cone–Plate measuring geometry, CP 25-2, having radius of 12.5 mm. Steady shear viscosity measurements were performed at various shear rates ranging from 0.005 to 100 s^{-1}. The gelation time was determined by measuring storage modulus (G') from dynamic stress sweep measurements. The data were fitted to rheological models of Cross, modified-Carreau and Carreau-Yasuda, which are special cases of Eq. 1, which take into account particle interactions in dispersed systems and can be applied for gelcasting systems [37].

$$\eta(\dot{\gamma}) = \eta_0[1 + (\lambda\dot{\gamma})^a]^{\frac{n-1}{a}} \quad (1)$$

where η_0 is the viscosity of an initial Newtonian region at low shear rates, a is the transition width parameter from initial Newtonian region to power law behavior and λ, a constant with unit time, expressing a characteristic time on the order of terminal relaxation time. In the Cross and modified-Carreau models a = 1–n and a = 1, respectively [37,38]. The value of a is considered variable in the Carreau-Yasuda model.

Samples were casted in 20 × 20 mm sheets and placed in SBF for 1 h at 37°C. Fully hydrated hydrogel weight (W_s) was recorded by blotting off the excess water. Then, hydrogels were freeze dried to − 40°C for 12 h to obtain the dry weigh (W_d). The equilibrium water content (EWC) was then calculated by

$$\mathrm{EWC}(\%) = \frac{W_s - W_d}{W_s} \times 100 \quad (2)$$

Dynamic shear stress sweeps were performed to investigate the storage moduli (G') and the loss moduli (G'') of the hydrated hydrogels. The tests were performed in a water bath at 37°C with a 25 mm parallel plate at a gap of 800 µm. The effects of the PEG molecular weight (600 and 900 Da) and Laponite particles on the shear properties were studied. Tensile tests were performed using a tensile tester employing a 100 N measuring cell under tensile loading with a cross-head speed of 5 mm/min. Five specimens for each composition were gelcasted to obtain 25 mm × 120 mm bars. After fully hydration for 1 h in SBF, the specimens were coated with silicone vacuum grease to minimize water loss during the test. The tensile loading was performed in a wet chamber at 37°C and 70% RH.

The microstructure of as-prepared hydrogels and fully hydrated hydrogels was studied by a VEGA3 SB-Tescan scanning electron microscopy (TESCAN, Czech Republic) at an accelerating voltage of 5 kV. Hydrogels were maintained in SBF at 37°C for 72 h and 14 days to study structural stability at the physiological conditions. All samples were freeze-dried at 15°C for 24 h, plunged in liquid nitrogen and then broken to attain the cross section. The samples were fixed on a metal stub with conductive tape and then coated with gold under vacuum by ion sputtering (Cressington, sputter coater 108 auto; thickness controller MTM-20) before SEM measurements.

2.5. Cell viability evaluation

The MTT assay was used to evaluate the cytotoxicity of hydrogels crosslinked by imide ring opening reaction. Human mesenchymal stem cells (hMSCs; Pasteur Institute, Iran) were utilized. The samples were sterilized by plasma irradiation for 30 min in a 24-well plate. The residual BDA was removed by washing the specimens by PBS for three times before incubation. The hMSCs (10^5 UCF) were seeded on the samples and incubated for 48 h at 37°C under 5% CO_2 atmosphere. After removing the medium, 50 µL of MTT was added to each well and immediately covered by aluminum foil to protect the solution from light. The wells were then incubated for 4 h at 37°C in 5% CO_2. The solution was removed and replaced by 200 µL of DMSO added to each well and incubated for another 20 min. The solution was mixed by pipette in order to completely wash out the salt from the samples. The solution of each well was transferred to three wells of a 96-well plate and then analyzed at wavelengths of 570 and 630 nm. The data were reported separately for each well by the ELISA reader machine (800 Biotek, USA), then an average of triplicate wells were calculated and normalized by dividing to the amount of the control well. For microscopic observations the samples were placed at the bottom of a 12-well culture plate and sterilized. The number of 20000 cells (with density of 5×10^{10} cells/mL^{-1}) were seeded on each well and placed in incubator at 37°C for seven days. The culture medium was discarded and hMSCs were washed with PBS twice following fixation by 4% glutaraldehyde solution and staining with 670 micromolar acridine orange (Sigma, USA).

2.6. Statistics

Data are presented as mean ± SD. At least three samples are represented for each datum point. Statistical comparisons were performed with one-way analysis of variance (ANOVA) and statistical significance for all tests was set at $p < 0.05$.

3. Results and discussion

3.1. Block copolymer precursor synthesis

A new synthetic approach was used to obtain the PEG-based copolymer with imide blocks. Figure 2 shows the GPC and ^{13}C-NMR spectra of the PEG-based copolymer with imide groups. The NMR peaks were determined by SDBS (http://sdbs.db.aist.go.jp). Typically, carbons (^{13}C) of the imide groups (-CO-N-CO-) gave a peak on ~166.1 ppm (Ca). Peaks in the ~136.5 ppm and ~117.1 ppm represent carbons of the benzene rings on the imide blocks (C_b, C_c). Peaks observed on about ~74 ppm (Cd), 69 ppm (Ce,f) represent the main chains of ethylene glycol. Finally, peaks of ~48 ppm (Cg),

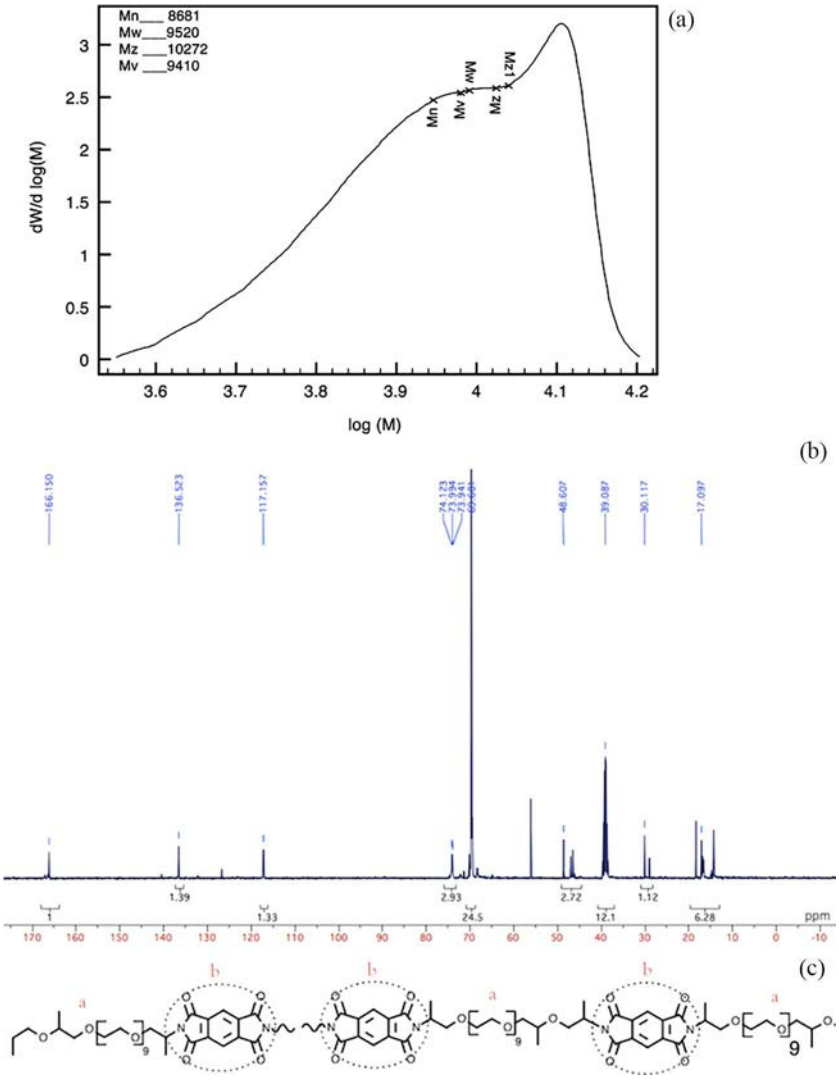

Figure 2. (a) GPC and (b) ^{13}C-NMR spectra for PEG-co-PMDA copolymers with multiple imide groups. (c) Schematic of the synthesized linear block copolymer.

~30 ppm (Ci), and ~17 ppm (Ch) corresponding to the carbons of the propylene oxide capping PEG chains (Figure 2b).

The introduction of imide groups into amino-terminated PEG (ATPEG) was carried out by thermal imidization following two different synthetic stages, as illustrated in Figure 1. At the first stage, anhydride groups of PMDA react with amine groups of ATPEG at 0°C to form a poly-(amic acid) during an exothermic reaction. During the second stage, intermediate amic acid was transformed to imide groups attached to a benzene ring via thermal treatment. Polyimide synthesis is highly controllable by the stoichiometric ratio by affecting the progress of poly-(amic acid) formation at the first stages of synthesis [39]. Side reactions are among other factors that may have a significant effect on the molecular weight (both M_w and M_n) and the polydispersity of the final product. Reverse propagation reaction of the poly-(amic acid) is an important side reaction that cannot be completely removed (Figure 1b). This intramolecular acidolysis is a result of the pendant carboxylic groups at the ortho positions [40]. The other important side reaction is that of the dianhydride with water, which also competes with the primary reaction. This reaction would have a dramatic effect on the molecular weight of the poly-(amic acid) as it removes the dianhydride from equilibrium and decreases the monomer stoichiometry [39,40]. To decrease the influence of side reactions, higher concentrations of the monomers along with a slight excess of dianhydride was used to attain higher molecular weights. The weight and weight distribution of the PEG-co-PMDA macromolecule were determined by GPC, as shown in Figure 2a. The molecular weight of the copolymer was about 10 kDa for both intermediate PEG600 and PEG900. In considering PDI, the number of active crosslinking sites (imide blocks, Figure 2c) for the copolymer derived from PEG600 and PEG900 was about 11 and 9, respectively.

3.2. Exfoliation of laponite particles in PEG-Co-PDMA copolymer

Laponite particles were added during the first stage of the polyimide synthesis. During this stage poly-(amic acid) can act similar to amino acid compatibilizing agents for clay particles. Namely, in the acidic medium, a proton is transferred from the –COOH group to the intramolecular $-NH_2$ group. A cation exchange is then possible between the $-NH_3^+$

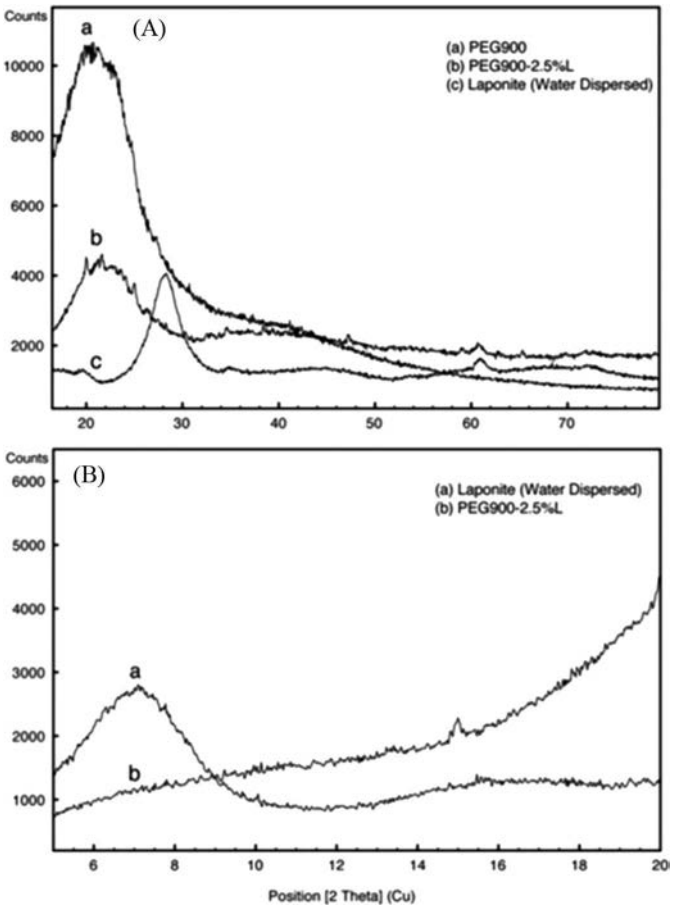

Figure 3. (A) Wide-angle XRD pattern of Laponite particles, PEG900 and PEG900-2.5%L. (B) Low-angle XRD pattern of Laponite and PEG900-2.5%L.

function formed and the Na^+ cation intercalated between the clay layers, so that the clay becomes organophilic. Organophilicity of the clay, obtained during the first stage, coupled with dipolar aprotic solvent acting at high temperature during the second stage, leads to highly exfoliated silicate layers dispersed in polymeric medium. XRD was used to investigate the role of imidization synthesis on the obtained structure of the Laponite particles. Figure 3a shows a wide-angle XRD pattern of Laponite particles in comparison with hydrogel discs made under compression during gel casting. For the water dispersed Laponite particles, the clay platelets formed a film with (*00 L*) basal plane oriented parallel to the substrate surface. Therefore, a diffraction pattern with highly oriented (*00 L*) diffraction peaks was attained while the two-dimensional (*hk0*) diffraction bands were reduced. The high-intensity diffraction peak at $2\theta = 6.94°$ corresponded to the (001) d-spacing of 12.73 Å referred to as the basal plane spacing [27]. Although particle orientation significantly reduced the intensity of lateral diffraction peaks by arranging them perpendicular to the substrate surface, a diffraction peak of (060) was observed at ~61° due to its high intensity [38]. No diffraction peaks were detected for pristine hydrogels, which indicated a completely amorphous structure of the copolymer. By comparing the diffraction pattern of nanocomposite hydrogel with that of the pristine hydrogel, (060) lateral planes (at ~61° 2θ) were visible. On the other hand, the (*00 L*) diffraction peaks were absent in both wide- and low- diffraction patterns (Figure 3b). This can be attributed to the particle exfoliation within the hydrogel medium during polyimide preparation, which eliminated the ordered laminated structure of Laponite and removed the basal plane spacing peaks [41].

The mechanism of particle exfoliation during synthesis can be explained by clay cation exchange processes during the polyimide synthesis [42]. A characteristic feature of montmorillonite is their ability to absorb certain cations and to retain them in an exchangeable state. It means that Na^+ cation can be exchanged by treatment of other cation in a polar solution. In this case, Na^+ cation can be exchanged by NH_3^+, which is formed during poly-(amic acid) formation of copolymer synthesis [43]. Zeta potential measurement was shown that the surface charge of the in-situ and *ex situ* (mixed) nanocomposites was $\xi_s = 45.7 \pm 4.2$ mV and $\xi_M = 27.3 \pm 3.7$ mV, respectively. Adsorption of organic cations to the clay particles beyond the cation exchange capacity (CEC) of the clay is mainly due to the high concentration of secondary cations, which drives the cation exchange equilibrium to exchange more NH_3^+ cations [44,45]. The higher zeta potential of the *in situ* composite is attributed to the additional hydrophobic interactions between the adsorbing cations and steric inhibition of poly-(amic acid) chains during *in situ* copolymerization that makes cation exchange easier by providing more diffusion space [46]. Furthermore, as the cation exchange is a diffusion control process, any parameter that improves

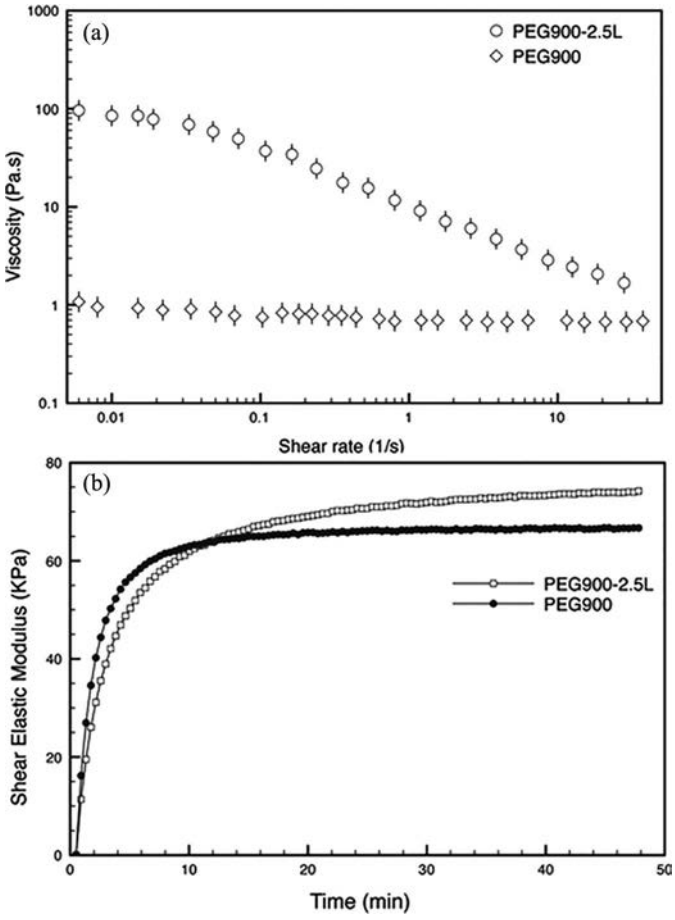

Figure 4. (a) Steady shear viscosity measurements of PEG900 with and without 2.5% Laponite nanoparticles at 30 wt% solid loading. (b) Gelation time.

Table 1. Model analysis of the rheological data for PEG900 hydrogel with and without 2.5% Laponite nanoparticle.

Model	a	n	λ (s)	η_0 (Pa.s)	Adj. R^2	RMSE
Cross	0.7474	0.2731	45	250	0.834	0.15
Modified Carreau	1	0.2723	45	250	0.9113	0.1
Carreau-Yasuda	3.08	0.2755	45	250	0.9885	0.03

diffusion rate of cations can improves cation exchange and consequently the surface charge of the particles.

3.3. Rheological behavior of injectable precursor solutions

As mentioned previously, injectable gels have several advantages over preformed implants, such as their noninvasive introduction *in vivo* and the ability to be used to homogeneously encapsulate cells and macromolecules. Therefore, studying the rheological properties of the copolymer is important. A shear thinning behavior that makes the precursor more viscous at low applied shear while the precursor solution can be easily injected applying a shear stress with a simple syringe [28] is desirable. Figure 4a shows the rheological behavior of as prepared precursors with a total solid loading of 30 wt%. As seen, the addition of Laponite particles increased the viscosity of precursor while changing its behavior from Newtonian to thixotropic. The physical and ionic interactions between polymer chains and Laponite surface restrict polymer chains mobility. Furthermore, matrix-allowing edge-to-face particle-particle interactions clay platelets form a "house of cards" structure at low shear rates and consequently increase the viscosity [47]. By increasing the shear rates, clay platelets may align with the applied stress that facilitate polymer mobility and decrease the viscosity at higher shear rates. The results of model analysis for the rheological data are reported in Table 1. RMSE and adjusted R^2 parameters show the deviation and adjustment of each fitted curve, respectively. It appeared that Carreau-Yasuda model could be used to predict the rheological properties of the nanocomposite while Newtonian behavior fitted the pristine PEG900 precursor. Therefore, the addition of Laponite provides advantages of shear thinning for injectable cartilage.

In addition to the shear thinning behavior, the gelation time is of vital importance for injectability. To study the gelation time, 1 g of PEG900 (without Laponite nanoclays) and PEG900-2.5%L (with 2.5 wt% Laponite nanoclays) were treated with a predetermined amount of BDA under oscillatory stress of 10 Pa and frequency of 0.1 Hz (Figure 4b). The gelation time of PEG900 and PEG900-2.5%L was approximately 13 and 27 min, respectively. The longer gelation time in the presence of Laponite particles could be attributed to lower cross linker diffusion rate caused by the aligned free surfaces of clay layers [48].

3.4. Mechanical properties of hydrogels

Oscillatory shear sweeps were performed from 0.1 to 1000 Pa with a frequency of 1 Hz to find the shear stress in which

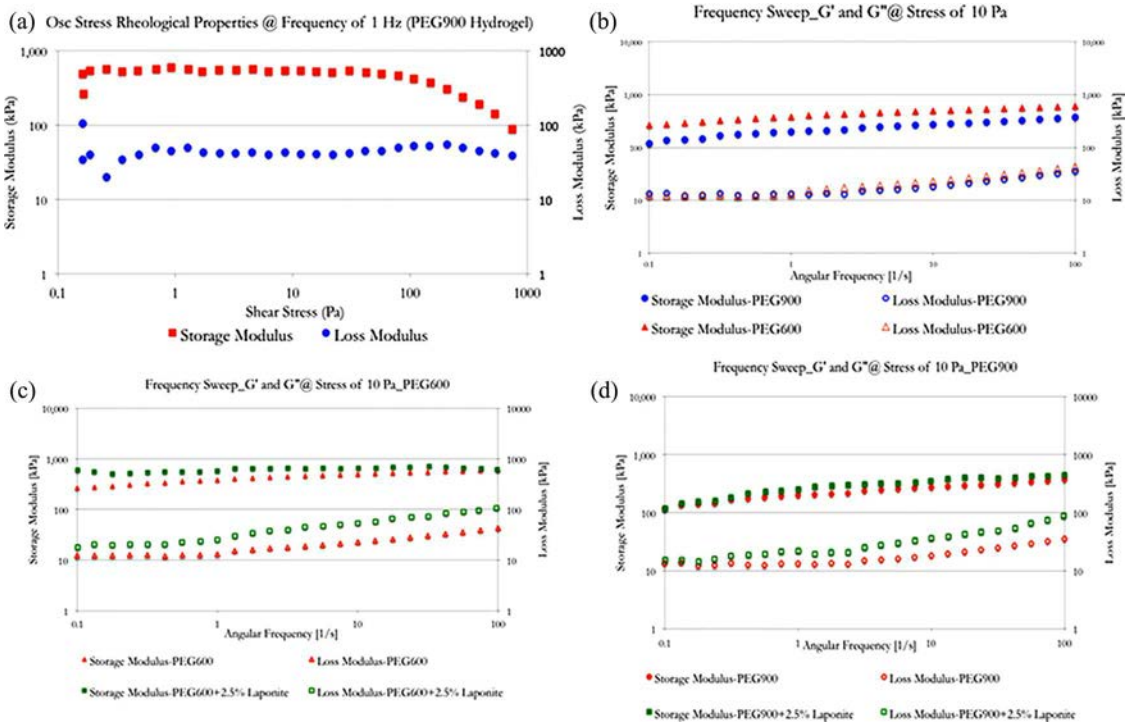

Figure 5. Storage modulus and loss modulus for the examined hydrogels. (a) Oscillatory shear sweeps were performed from 0.1 to 1000 Pa with a frequency of 1 Hz. (b) Elastic and viscous modulus of PEG600 and PEG900 hydrogels at a constant applied stress of 10 Pa. (c,d) Effect of shear stress at a constant frequency of 1 Hz on the shear behavior of PEG600 and PEG 900 hydrogel with or without Laponite particles.

samples exhibit linear viscoelastic behavior (Figure 5a). Elastic moduli (G') and the viscous moduli (G") were calculated at a shear stress of 10 Pa and frequencies of 0.1–100 Hz. Figure 5b indicates that the elastic modulus of PEG600 hydrogel is higher than that of PEG900 while their viscous moduli are relatively close. The higher number of crosslinking sites in the polymer chain of PEG600 enhances its viscous moduli as compared to PEG900, as explained by [49]:

$$G = NkT\frac{r^2{}_i}{r^2{}_o} \tag{3}$$

$r^2{}_o$ is the chains' mean-square end-to-end distance when they are unaffected by crosslinks and $r^2{}_i$ is the mean square average over the assembled chains crosslinked into the network. N is the number of subchains per unit volume.

Figures 5c and 5d show the shear modulus of PEG and PEG-based nanocomposites. The addition of clay nanoparticles not only improved the elastic modulus of hydrogels by more than 20%, but also enhanced the viscous modulus more than 50% at each frequency. The results confirmed that the enhancement of crosslinking density along with introduction of exfoliated silicate layers successfully improved the shear modulus of the synthetic hydrogel. It is also noteworthy that, the attained shear modulus is close to the shear modulus of collagen ECM in animal models (380–650 kPa) [50] and higher than the most of the current hydrogels as a scaffold for type II collagen seeding [3]. In addition, the results have a good compliance with the measured dynamic modulus of human lateral condyle [51]. Under shear stress, the polymer chains reversibly adsorb and desorb onto the charged silicate surfaces while adopting trains and loops conformations [52,53]; hence, the viscous modulus of the hydrogel composite is enhanced compared to the pristine PEG hydrogels.

Engineering stress-strain curves of the studied hydrogels are shown in Figure 6a. The hydrogels exhibited an elastic region followed by a stress drop after yielding (Figure 6a). The higher elastic modulus of PEG600 is due to more crosslinking sites in a single chain. The addition of Laponite (2.5%) increased the Young modulus by about 20% through physical crosslinking. The stress drop is attributed to strain softening and simultaneous localized necking. It is also observed that the stress-strain curves in the plastic deformation region are noisy and serrated, which may be attribute to the stress intensification and relief after necking [54]. Further deformation was accompanied with elimination of crosslinked sites and network fracture. The results also revealed that the addition of Laponite nanolayers dramatically increased the yield strength of the hydrogels due to the physical crosslinking, that is, adsorption of NH_3^+ ions during the *in situ* synthesis lead to the formation of crosslinking sites on the Laponite surfaces, which improved the yield stress by making chemical linking sites harder to detach. On the other hand, elongation was decreased by the clay nanoparticles as the

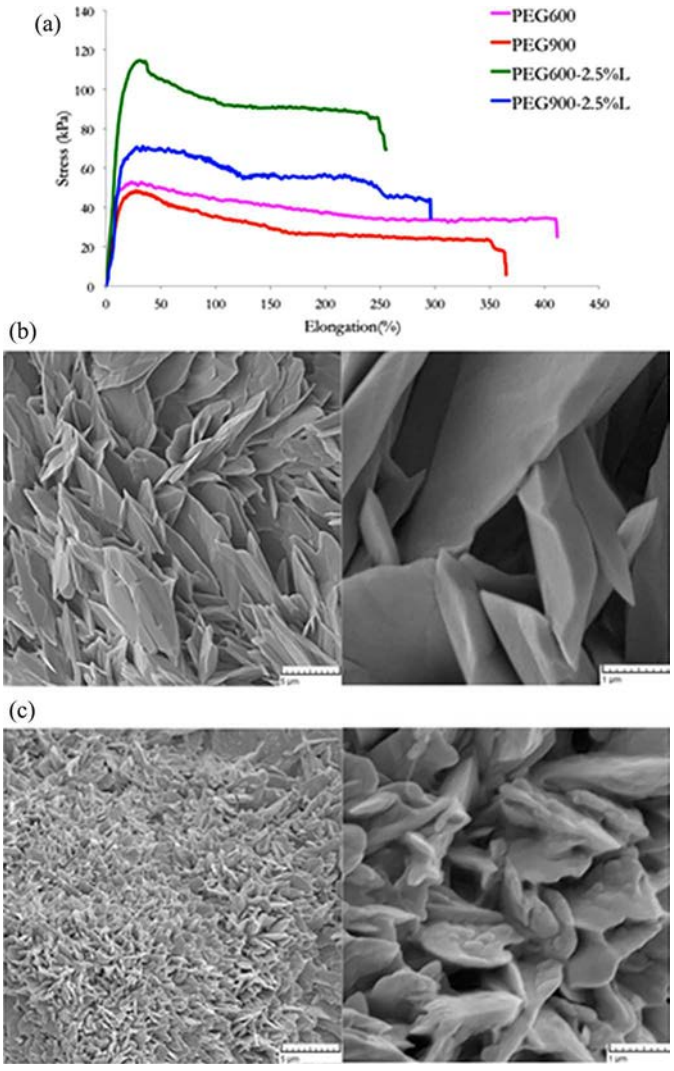

Figure 6. Tensile behavior of PEG-based hydrogels. SEM images show the microstructure of PEG900 hydrogels (b) without and (c) with 2.5% Laponite. The images indicate the formation of stacked structures in the nanocomposites.

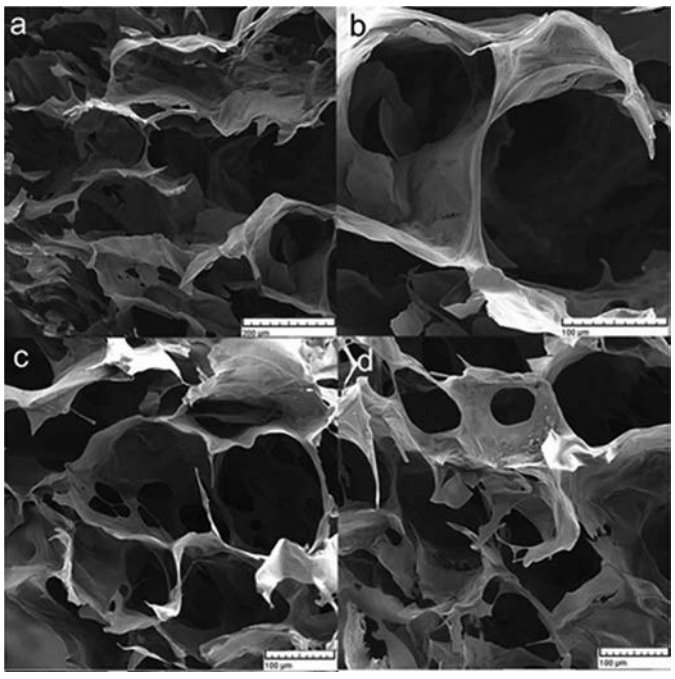

Figure 7. SEM images showing the pore structure of (a,b) PEG900 and (c,d) PEG900-2.5%L hydrogels incubated for 72 h in SBF at 37°C. (d) 3D image of the interconnected porosity by confocal electron microscopy.

nanolayers formed upon processing (see Figures 6b and 6c) could operate as Griffith cracks and a source of stress concentration. In fact, the formation of flaky structures with an average thickness of < 0.1 μm remarkably changed the deformation behavior of the nanocomposites. This type of structures has also recently been reported by Nelson and Cosgrove [52]. They have shown that polymer chains adsorb to the Laponite surface, while adopting loop and train conformations, making a polymer layer on the silicate surface with the hydrodynamic thickness between 20 and 160 nm.

3.5. Microstructure of hydrogels in physiological environment

Scanning electron microscopy (SEM) was employed to study the microstructure of the prepared hydrogels after five days of incubation in simulated body fluid (SBF). Figure 7 shows SEM image of the pore structure of PEG900 hydrogel without and with Laponite particles. The pores are fully interconnected with sizes in the range of 100–200 μm, which is well suited for differentiation and proliferation of cells within a cartilage scaffold [55].

Figure 8 shows the equilibrium water content (EWC) for different samples. EWC changes were observed by adding Laponite clay particles or changing the MW of precursor chains. The reason can be attribute to the ionic induced entanglements at the surface of clay particles, which limits the ability of hydrogen bonding on the PEG chains. Furthermore, longer chains induce higher water affinity due to the lower crosslinking density and longer free chains. Thus, samples with Laponite particles and higher crosslinking density exhibit excellent swelling ratio (~80%), similar to the superficial zone of natural articular cartilage, which is the most susceptible part to damage [56].

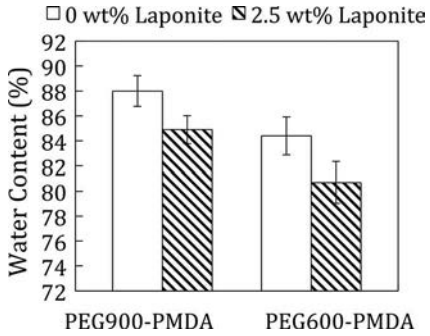

Figure 8. Effect of nanoclay particles on the equilibrium water content of PEG-based hydrogels.

3.6. Cell viability

Figure 9a shows the results of MTT assay performed on hydrogels. It was found that that the cell viability was >80% for all hydrogels, indicating biocompatibility of the materials. Meanwhile, purification of the hydrogels by removing excess BDA improved the cell viability by 5–15%. Although the amount of utilized BDA for network crosslinking was significantly lower than the toxic level of putrescine [57], diffusion of BDA across the cell membrane and trapping inside the cells, even at low concentrations, could impair cell viability assay. It was also found that the cell viability of PEG900 hydrogel was more than PEG600, mainly due to lower BDA concentration. On the other hand, the addition of Laponite layers slightly decreased the cell viability of the scaffolds, which could be attributed to the role of these layers on the entrapment of BDA molecules by ionic bonding. Fluorescent images of viable isolated hMSCs in the vicinity of the samples after 14 days of cell culture are shown in Figures 9b and 9c, which confirms the cell viability tests from MTT assay.

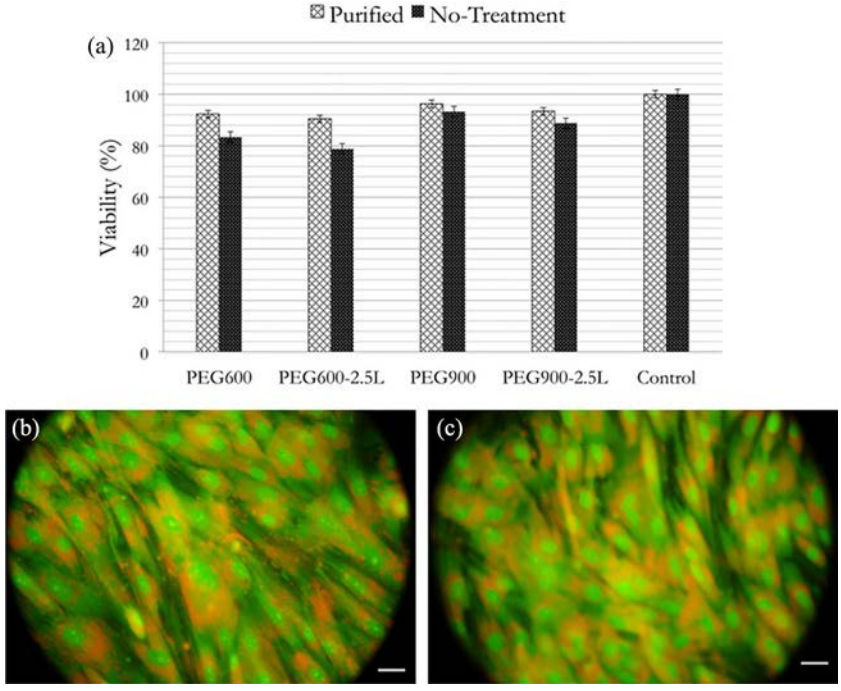

Figure 9. Fluorescent images of viable isolated hMSC in the vicinity of the samples after 14 days of cell culture at 5×10^{10} cells·mL^{-1} (scale bar = 20 μm).

4. Conclusions

PEG chains with multiple maleimide groups as active sites were synthesized via thermal imidization. It was found that a high density of hydrophilic crosslinking sites significantly increased the elastic modulus of the hydrogels compared with conventional PEG hydrogels. On the other hand, *in situ* synthesis of PEG-based hydrogels containing Laponite nanoparticles caused exfoliation of the silicate layers by the hydrogel network. Evaluation of the rheological behavior and gelation time of the hydrogels indicated a change from Newtonian flow behavior to thixotropic shear thinning via clay addition. Uniaxial tensile testing and oscillatory shear stress assay also showed enhanced elastic modulus of the PEG-based hydrogels by the addition of the Laponite nanoparticles. The viscous modulus was improved by about 50%, making the viscoelastic properties of the obtained hydrogels close to those reported for articular cartilage in animal models (380–650 KPa). Cell viability tests by hMSC indicated biocompatibity of the PEG hydrogels. Although the addition of Laponite particles slightly decreased the cell viability, the nanocomposite hydrogels exhibited reasonable biocompatibility (>90%). Meanwhile, *in vivo* investigations are required to assay the potential of the hydrogel in animal models.

References

[1] Fox, S. A.; Bedi, A.; Rodeo, S. *Sports Health* **2009**, *1*, 461.
[2] Annabi, N.; Nichol, J. W.; Zhong, X.; Ji, C.; Koshy, S.; Khademhosseini, A.; Dehghani, F. *Tissue Eng.* **2010**, *16*, 371.
[3] Bryant, S. J.; Anseth, K. S. *J. Biomed. Mater. Res.* **2001**, *59*, 63.
[4] Bryant, S. J.; Anseth, K. S. *J. Biomed. Mater. Res.* **2003**, *64*, 70.
[5] Bryant, S. J.; Anseth, K. S.; Lee, D.; Bader, D. L. *J. Orthopaed. Res.* **2004**, *22*, 1143.
[6] Pasut, G.; Veronese, F. M. *Prog. Polym. Sci.* **2007**, *32*, 933.
[7] Levitsky, J.; Fiel, M. I.; Norvell, J. P.; Wang, E.; Watt, K. D.; Curry, M. P.; Tewani, S.; McCashland, T. M. *Gastroenterology* **2012**, *142*, 1132.
[8] Drury, J. L.; Mooney, D. J. *Biomaterials* **2003**, *24*, 4337.
[9] Pedron, S.; Peinado, C.; Bosch, P.; Anseth, K. S. *Acta Biomater.* **2010**, *6*, 4189.
[10] Shao, L.; Chung, T. S.; Goh, S. H.; Pramoda, K. P. *J. Membr. Sci.* **2004**, *238*, 153.
[11] Sun, J.; Wang, Y.; Dou, S.; Ruan, C.; Hu, C. *Mater. Lett.* **2012**, *67*, 215.
[12] Powell, C. E.; Duthie, X. J.; Kentish, S. E.; Qiao, G. G.; Stevens, G. W. *J. Membr. Sci.* **2007**, *291*, 199.
[13] Ryan, S.; Mantovani, G.; Wang, X.; Haddleton, D.; Brayden, D. *Expert Opin. Drug Deliv.* **2008**, *5*, 371.
[14] Fogaça, R.; Catalani, L. H. *Soft Mater.* **2013**, *11*, 61.
[15] Li, Y.; Yang, C.; Khan, M.; Liu, S.; Hedrick, J. L.; Yang, Y. *Biomaterials* **2012**, *33*, 6533.
[16] Kopecek, J. *Biomaterials* **2007**, *28*, 5185.
[17] Hench, L. L. *J. Eur. Ceram. Soc.* **2009**, *29*, 1257.
[18] Bhattacharyya, S.; Guillot, S.; Dabboue, H.; Tranchant, J. F.; Salvetat, J. P. *Biomacromolecules* **2008**, *9*, 505.
[19] Paxton, J. Z.; Donnelly, K., Keatch, R. P.; Baar, K. *Tissue Eng.* **2009**, *15*, 1201.
[20] Chang, C. W.; Van Spreeuwel, A.; Zhang, C.; Varghese, S. *Soft Matter* **2010**, *6*, 5157.
[21] Schexnailder, P.; Schmidt, G. *Colloid. Polym. Sci.* **2009**, *287*, 1.
[22] Haraguchi, K. *Polym. J.* **2011**, *43*, 223.
[23] Nelson, A.; Cosgrove, T. *Langmuir* **2004**, *20*, 10382.
[24] Nelson, A.; Cosgrove, T. *Langmuir* **2004**, *20*, 2298.
[25] Gaharwar, A. K.; Rivera, C. P.; Wu, C. J.; Schmidt, G. *Acta Biomater.* **2011**, *7*, 4139.
[26] Gaharwar, A. K.; Schexnailder, P. J.; Kline, B.; Schmidt, G. *Acta Biomater.* **2011**, *7*, 568.
[27] Kornmann, X. *Synthesis and Characterisation of Thermoset-Clay Nanocomposites*; Luleå University of Technology, Luleå, Sweden, 1999.
[28] Geisler, I. M.; Schneider, J. P. *Adv. Funct. Mater.* **2012**, *22*, 529.
[29] Hoppe, A.; Güldal, N. S.; Boccaccini, A. R. *Biomaterials* **2011**, *32*, 2757.
[30] Capito, R. M.; Azevedo, H. S.; Velichko, Y. S.; Mata, A.; Stupp, S. I. *Science* **2008**, *319*, 1812.
[31] Wang, S.; Nagrath, D.; Chen, P. C.; Berthiaume, F.; Yarmush, M. L. *Tissue Eng.* **2008**, *14*, 227.
[32] Toledano, S.; Williams, R. J.; Jayawarna, V.; Ulijn, R. V. *J. Am. Chem. Soc.* **2006**, *128*, 1070.
[33] Li, Q.; Wang, J.; Shahani, S.; Sun, D. D. N.; Sharma, B.; Elisseeff, J. H.; Leong, K. W. *Biomaterials* **2006**, *27*, 1027.
[34] Yan, C.; Altunbas, A.; Yucel, T.; Nagarkar, R. P.; Schneiderk, P. *Soft Matter* **2010**, *6*, 5143.
[35] Peters, T. J. *All About Albumin. Biochemistry, Genetics, and Medical Applications*; Academic Press, San Diego, CA, 1996.
[36] Baukal, C. E. Jr.; Gershtein, V.; Li, X. J. *Computational Fluid Dynamics in Industrial Combustion*; CRC Press, Boca Raton, FL, 2001.
[37] Kühnle, H. *Int. Polym. Proc.* **1987**, *1*, 116.
[38] Nojoomi, A.; Faghihi, M. A.; Khoshkalam, M. *Ceram. Int.* **2014**, *40*, 123.
[39] Takekoshi, T.; Ghosh, M. K.; Mittal, K. L. *Polyimides- Fundamentals and Applications*; CRC Press, New York, 1996.
[40] Zeng, C.; Seino, H.; Ren, J.; Hatanaka, K.; Yoshie, N. *Polymer* **2013**, *54*, 5351.
[41] Blanton, T. N.; Majumdar, D.; Melpolder, S. M. *Adv. X-Ray Anal.* **2000**, *42*, 562.
[42] Ke, Y. C.; Stroeve, P. *Polymer-Layered Silicate and Silica Nanocomposites*, 1st edn.; Elsevier, Amsterdam, the Netherlands, 2005.
[43] Lan, T.; Kaviratna, P. D.; Pinnavaia, T. J. *Chem. Mater.* **1997**, *7*, 2144.
[44] Aochi, Y. O.; Farmer, W. J. *Colloids Surf. A* **2011**, *374*, 22.
[45] Blachier, C.; Michot, L.; Bihannic, I.; Barrès, O.; Jacquet, A.; Mosquet, M. *J. Colloid Interface Sci.* **2009**, *336*, 599.
[46] Zadaka, D.; Radian, A.; Mishael, Y. G. *J. Colloid Interface Sci.* **2010**, *352*, 171.
[47] Li, J.; Zhou, C.; Wang, G.; Zhao, D. *J. Appl. Polym. Sci.* **2003**, *89*, 3609.
[48] Kuo, C. K.; Ma, P. X. *Biomaterials* **2001**, *22*, 511.
[49] McCrum, N. G.; Buckley, C. P.; Bucknall, C. B. *Principles of Polymer Engineering*; Oxford University Press, New York, 1988.
[50] Arokoski, J. P. A.; Hyttinen, M. M.; Helminen, H. J.; Jurvelin, J. S. *J. Biomed. Mater. Res.* **1999**, *48*, 99.
[51] Fakult, M.; Ronken, S. *Dynamic stiffness of articular cartilage and potential repair materials*; PhD thesis, University of Basel, **2012**.
[52] Nelson, A.; Cosgove, T. *Langmuir* **2004**, *20*, 1382.
[53] Loizou, E.; Butler, P.; Porcar, L.; Kesselman, E.; Talmon, Y.; Dundigalla, A. *Macromolecules* **2005**, *38*, 2047.
[54] Wu, P. D.; Van der Giessen, E. *Int. J. Plast.* **1995**, *11*, 211.
[55] Lien, S. M.; Ko, L. Y.; Huang, T. J. *Acta Biomater.* **2009**, *5*, 670.
[56] Buckwalter, J. A.; Mankin, H. J. *J. Bone Joint Surg Am.* **1997**, *79*, 600–611.
[57] Guarino, L. A.; Cohen, S. S. *Proc. Natl. Acad. Sci. U S A* **1979**, *76*, 3660.